Detecting radiances in the O2 A band using polarization sensitive satellite instruments with application to Global Ozone Monitoring Instrument

Stam, D.M.; de Haan, J.F.; Hovenier, J.W.; Aben, I.

published in
Journal of Geophysical Research. Atmospheres
2000

DOI (link to publisher)
10.1029/2000JD900313

document version
Publisher's PDF, also known as Version of record

JOURNAL OF GEOPHYSICAL RESEARCH, VOL. 105, NO. D17, PAGES 22,379–22,392, SEPTEMBER 16, 2000

Detecting radiances in the O_2 A band using polarization-sensitive satellite instruments with application to the Global Ozone Monitoring Experiment

D. M. Stam[1]

Space Research Organization Netherlands, Utrecht

Department of Physics and Astronomy, Vrije Universiteit, Amsterdam, The Netherlands

J. F. De Haan and J. W. Hovenier[2]

Department of Physics and Astronomy, Vrije Universiteit, Amsterdam, The Netherlands

I. Aben

Space Research Organization Netherlands, Utrecht

Abstract. In this paper, we present numerical simulations of the radiance and the degree of linear polarization of light reflected by the terrestrial atmosphere in the O_2 A absorption band, around 760 nm. Since the O_2 A band is often used to derive cloud parameters, we included clouds in our model atmosphere. The simulations show that the polarization of the reflected light changes across the O_2 A band, and that this change depends strongly on the spectral resolution of the instrument. The polarization of reflected light induces errors in radiances derived from observations by polarization sensitive instruments. For the Global Ozone Monitoring Experiment (GOME) satellite instrument, which measures radiances with about 0.4-nm spectral resolution in the O_2 A band, broadband polarization measurements are used to correct the narrowband radiance observations for the instrument's polarization sensitivity. Although such correction schemes significantly improve the accuracy of derived radiances in the continuum, they do not account for changes of the polarization in narrow absorption bands, such as the O_2 A band. The main purpose of this paper is to investigate for cloudy atmospheres the errors in the derived radiances due to polarization changes across the O_2 A band, both for a polarization sensitive instrument with a high spectral resolution and for a GOME-like resolution. If no correction scheme is used, it is found that for nadir viewing directions, the maximum errors in the absorption band can increase by up to about 20% with decreasing width of the spectral response function when the instrument's sensitivity for radiation polarized perpendicularly to the principal plane is twice as large as that for radiation polarized parallel to this plane. If, in this case, a correction scheme based on the broadband value of the polarization is used, the radiance errors can still be up to 18% with a high spectral resolution and of the order of a few percent with a GOME-like resolution.

1. Introduction

The oxygen (O_2) A absorption band plays an important role in remote sensing of the terrestrial atmosphere from space. The interest in applications of this absorption band mainly arose when *Hanel* [1961] proposed to derive the vertical column density of a well-mixed gas above a cloud deck, and thus the cloud top altitude, from comparing radiances of light reflected by the cloud at wavelengths inside an absorption band of the gas with radiances of reflected light measured at nearby wavelengths outside the band. Hanel suggested using the CO_2 absorption band at 2.0 μm. However, as was pointed out by *Yamamoto and Wark* [1961], the O_2 A band, between 750 and 780 nm, appeared to be preferable. Because cloud top altitude is an important parameter both for climatological and meteo-

[1]Now at Astronomy Department, Cornell University, Ithaca, New York.

[2]Also at Astronomical Institute Anton Pannekoek, University of Amsterdam, Amsterdam, The Netherlands.

Paper number 2000JD900313.
0148-0227/00/2000JD900313$09.00

rological research and for the interpretation of satellite measurements, a considerable number of studies on the derivation of cloud top altitudes from radiances in the O_2 A band have been presented since then. Theoretical studies have been performed by, for example, *Wark and Mercer* [1965], *Fischer and Grassl* [1991], and *O'Brien and Mitchell* [1992]. Comparisons between theory and aircraft or satellite measurements have been published by, for example, *Saiedy et al.* [1967], *Wu* [1985], *Fischer et al.* [1991], and recently by *Vanbauce et al.* [1998].

The above mentioned studies show that the use of reflected radiances in the O_2 A band is a promising technique for deriving cloud top altitudes. In addition, it appears that the reflected radiances also depend on other atmospheric parameters, such as the cloud optical thickness, cloud geometrical thickness, the microphysical properties of the cloud particles, the atmospheric aerosol, and the surface reflection (see *Fischer and Grassl* [1991] for a comprehensive sensitivity study). Obviously, the O_2 A band is a powerful tool for remote sensing. Therefore it is not surprising that many satellite instruments have been equipped with one or more channels covering this absorption band. Examples of such instruments are Polarization and Directionality of Earth's Reflectance (POLDER) [*Deschamps et al.,* 1994] (POLDER 1 was launched in 1996 on the National Space Development Agency of Japan's first Advanced Earth Observing Satellite (ADEOS 1); POLDER 2 will be launched on ADEOS 2 in 2000); Global Imager (GLI) (on ADEOS 2); Medium Resolution Imaging Spectrometer (MERIS) (will be launched in 2001 on the European Space Agency's (ESA) first Environmental Satellite (Envisat 1)); Profiling A-Band Spectrometer/Visible Imager (PABSI) (will be part of NASA's CloudSat mission, scheduled for launch in 2003); Global Ozone Monitoring Experiment (GOME) (GOME 1 has been launched on ESA's second European Remote Sensing satellite (ERS 2) in 1995, GOME 2 will fly in 2002 on the first Meteorological Operational satellite (METOP 1)); and Scanning Imaging Absorption Spectrometer for Atmospheric Chartography (SCIAMACHY) (on Envisat 1).

The accuracy with which atmospheric parameters can be determined is limited by the accuracy of the radiances derived from the spectrometer's signals. Errors in these radiances might arise owing to the use of a polarization sensitive spectrometer, whose signals not only depend on the radiance of the observed light, but also on its state of polarization. In such a case, the state of polarization of the observed light should be known to accurately derive radiances from the measured signals.

The state of polarization of light emerging from the atmosphere also depends, besides on the illumination and viewing geometries, in general, on the atmospheric parameters mentioned before, on the surface reflection, and on the wavelength. Regarding the O_2 A band wavelength region, observations [*Stammes et al.,* 1994; *Preusker et al.,* 1995; *Aben et al.,* 1999] and numerical simulations [*Stam et al.,* 2000, 1999] have shown that without clouds, the degree of linear polarization of light diffusely transmitted through the atmosphere inside the absorption band can deviate significantly from that in the nearby continuum. Numerical results presented in this paper, show a similar pattern in the degree of linear polarization across the O_2 A band for light reflected by a cloudy atmosphere.

The main purpose of this paper is to investigate for the O_2 A band wavelength region the errors in the radiances derived from observations by polarization sensitive satellite instruments due to the wavelength dependence of the degree of linear polarization across the absorption band. To this end, we simulate both the radiance and the degree of polarization of the light reflected by a cloudy atmosphere, the instrument's signal, and the radiance derived from that signal. The signal not only depends on the instrument's polarization sensitivity, but also on the width and shape of the instrumental spectral response function (the "slit function"). The error in the radiance that is derived from the signal depends on what is known about the state of polarization of the observed light (assuming that accurate values of the instrumental parameters, such as the polarization sensitivity, are available).

We simulate signals both for a Dirac delta function like instrumental response function, and for a response function that is representative for the Global Ozone Monitoring Experiment (GOME) [*European Space Agency (ESA),* 1995; *Burrows et al.,* 1999] spectrometer on board the European Space Agency's ERS 2 satellite. The GOME instrument is a scaled-down version of SCIAMACHY [*Burrows et al.,* 1988], which will fly on ESA's Envisat 1 satellite. GOME is designed to measure both the solar irradiance and the radiance of sunlight reflected by the Earth from 240 to 790 nm, with a spectral resolution of 0.2 to 0.4 nm [*ESA,* 1995]. Both GOME and SCIAMACHY are polarization sensitive. For both instruments, the O_2 A band is an important wavelength region for the determination of cloud properties [*Kuze and Chance,* 1994] and other atmospheric parameters. Therefore it is important to assess the magnitude of the radiance errors in this band.

The errors in the radiances are derived both for the case in which the observed light is assumed to be unpolarized and for the case in which a constant degree and orientation of linear polarization across the absorption band are assumed. The latter case applies to GOME and SCIAMACHY, which have been equipped with broadband detectors known as polarization measuring devices (PMD) (see section 2.3).

The outline of this paper is as follows. In section 2, we give a description of radiance and polarization observations both for polarization insensitive and polarization sensitive instruments. In section 3, the atmospheric model and the radiative transfer calculations used for the simulations are described. In section 4, we present simulated radiance and polarization observations and

consider the errors in radiances derived from such simulated observations. Section 5 contains the discussion.

2. Detecting Radiances and Polarization

2.1. Stokes Parameters and Polarization

The radiance and state of polarization of light with wavelength λ can be described by a Stokes vector [*Chandrasekhar,* 1950; *Hovenier and Van der Mee,* 1983] as follows:

$$\mathbf{I}(\lambda) = \begin{bmatrix} I(\lambda) \\ Q(\lambda) \\ U(\lambda) \\ V(\lambda) \end{bmatrix}. \quad (1)$$

Stokes parameter I is the radiance of the light, Q and U describe the linearly polarized radiation, and V describes the circularly polarized radiation. All Stokes parameters have the dimension of radiance. Stokes parameters Q and U are defined with respect to a reference plane. In this paper, the principal plane, which contains both the vertical direction and the direction of propagation of the incoming sunlight, is chosen as the reference plane. Since the model atmosphere we use in our radiative transfer calculations is rotationally symmetric with respect to the vertical direction and the incident light is unpolarized, Stokes parameters U and V of the reflected light are equal to zero with respect to the reference plane. In our radiative transfer calculations, parameter V will be ignored. Considering calculations of Stokes parameters I and Q in the principal plane, we found that neglecting V introduces no errors in the calculated Stokes parameter I. The error in Q due to neglecting V was found to be smaller than 0.02% for solar zenith angles near 60° and to decrease with decreasing solar zenith angle.

The signal $J_{\rm ch}$, which would be detected in a channel of an ideal (i.e., polarization insensitive) radiance measuring instrument, can be written as

$$J_{\rm ch} = a_{\rm ch} \int_{\lambda_{\rm min}}^{\lambda_{\rm max}} S(\lambda) I(\lambda) d\lambda \doteq a_{\rm ch} I_{\rm ch}. \quad (2)$$

Here I is the radiance of the incident light, $a_{\rm ch}$ is the channel's response, and $\lambda_{\rm min}$ and $\lambda_{\rm max}$ bound the wavelength region across which the channel's spectral response function S deviates significantly from zero. The function S is normalized according to

$$\int_{\lambda_{\rm min}}^{\lambda_{\rm max}} S(\lambda) d\lambda = \lambda_{\rm max} - \lambda_{\rm min}. \quad (3)$$

Provided that $a_{\rm ch}$ is known, the observed radiance can be derived from the measured signal according to $I_{\rm ch} = J_{\rm ch}/a_{\rm ch}$.

Like the observed radiance $I_{\rm ch}$, we can also introduce $Q_{\rm ch}$ and $U_{\rm ch}$, for observed Stokes parameters Q and U, respectively, using the same $a_{\rm ch}$. The degree of linear polarization of the observed light is usually defined as $\sqrt{Q_{\rm ch}^2 + U_{\rm ch}^2}/I_{\rm ch}$. Since in our calculated Stokes vectors U (and thus $U_{\rm ch}$) is equal to zero, the definition for the degree of linear polarization we will use is the following:

$$P_{\rm ch} = -\frac{Q_{\rm ch}}{I_{\rm ch}}. \quad (4)$$

For the case $P_{\rm ch} > 0$, the observed light is polarized perpendicularly to the principal plane, and if $P_{\rm ch} < 0$, the direction of polarization is parallel to this plane.

2.2. Spectral Resolution

Considering observations in gaseous absorption bands where $\mathbf{I}$ varies rapidly with wavelength, like in the O_2 A band, $I_{\rm ch}$, $Q_{\rm ch}$, and $U_{\rm ch}$ depend strongly on the channel's spectral response function S. Therefore in this paper, we simulate observations performed with an instrument with S described by a Dirac delta function and observations performed with an instrument with a Gaussian-shaped response function that is representative for the GOME instrument [*ESA,* 1995].

An instrumental spectral response function that is shaped like a Dirac delta function represents an extreme case. Such a high spectral resolution offers the possibility to observe the shape of individual absorption lines.

The GOME-like response function is for each instrumental channel described by

$$S(\lambda) = B \exp\left(\frac{-(\lambda - \lambda_{\rm ch})^2}{2\sigma^2}\right). \quad (5)$$

Here B is a normalization constant, $\lambda_{\rm ch}$ is the wavelength at which the response is maximal, and $\sigma\sqrt{\ln 256}$ denotes the full width at half maximum of the response function and is assumed to be channel independent. In the O_2 A band wavelength region, we take $\sigma = 0.15$ nm and a distance of 0.2 nm between two successive values of $\lambda_{\rm ch}$ [*ESA,* 1995]. Truncating S at δ% of its maximum value and using equation (3) lead to

$$B = \frac{2\sqrt{\ln 100 - \ln \delta}}{\sqrt{\pi}\,\mathrm{erf}(\sqrt{\ln 100 - \ln \delta})}, \quad (6)$$

where $\mathrm{erf}(x) = (2/\sqrt{\pi}) \int_0^x \exp(-t^2) dt$. For our simulations, we assume $\delta = 1$. In the O_2 A band, each GOME-like instrumental channel covers a number of individual absorption lines.

2.3. Polarization Sensitive Instruments

In section 2.1, we introduced an ideal radiance measuring instrument. In reality, however, many instruments, such as GOME and SCIAMACHY, are sensitive to the degree and the direction of polarization of the incident light. When such an instrument observes light in the principal plane, and assuming the opening slit of the instrument to be oriented parallel to this plane, the signal measured in a channel can be written as

$$J_{\rm ch} = \frac{1}{2}a^l_{\rm ch}\int_{\lambda_{\rm min}}^{\lambda_{\rm max}} S(\lambda)\,[I(\lambda)+Q(\lambda)]\,d\lambda + \frac{1}{2}a^r_{\rm ch}\int_{\lambda_{\rm min}}^{\lambda_{\rm max}} S(\lambda)\,[I(\lambda)-Q(\lambda)]\,d\lambda \doteq \frac{1}{2}a^l_{\rm ch}\,[(1+\eta_{\rm ch})I_{\rm ch}+(1-\eta_{\rm ch})Q_{\rm ch}]. \quad (7)$$

Here $a^r_{\rm ch}$ denotes the channel's response to light polarized perpendicularly to the principal plane, $a^l_{\rm ch}$ is its response to parallel polarized light, and $\eta_{\rm ch} = a^r_{\rm ch}/a^l_{\rm ch}$. This $\eta_{\rm ch}$ represents the channel's polarization sensitivity. Note that for a polarization insensitive instrument, $\eta_{\rm ch} = 1$ and $a^l_{\rm ch} = a^r_{\rm ch} = a_{\rm ch}$, thus transforming equation (7) into equation (2).

From equation (7) it can be seen that for a polarization sensitive instrument, the radiance $I_{\rm ch}$ can be derived from the measured signal $J_{\rm ch}$ only when $\eta_{\rm ch}$, $a^l_{\rm ch}$, and $Q_{\rm ch}$ are known. Namely,

$$I_{\rm ch} = \frac{2}{a^l_{\rm ch}(1+\eta_{\rm ch})}J_{\rm ch} - \frac{(1-\eta_{\rm ch})}{(1+\eta_{\rm ch})}Q_{\rm ch}. \quad (8)$$

Since $\eta_{\rm ch}$ and $a^l_{\rm ch}$ are instrumental parameters, they can in principle be measured. As an example, Figure 1 shows $\eta_{\rm ch}$ of GOME for the channels between 580 and 800 nm as measured during the preflight calibration of the instrument [*Netherlands Organization for Applied Scientific Research - Institute of Applied Physics (TNO-TPD),* 1994]. Across these 1024 channels of GOME, $\eta_{\rm ch}$ can be seen to vary between 0.5 and 2.5. Like the radiance I, Stokes parameter Q of light reflected by Earth also depends, besides on wavelength, on atmospheric parameters, the surface reflectivity, and the illumination and viewing geometries. In the wavelength region containing the O_2 A absorption band, probably the best way to estimate $Q_{\rm ch}$ pertaining to the observed scene is to perform measurements. If there is no accurate knowledge on $Q_{\rm ch}$ available and a value $Q'_{\rm ch}$ is assumed, the radiance $I'_{\rm ch}$ that is derived from $J_{\rm ch}$ according to

$$I'_{\rm ch} = \frac{2}{a^l_{\rm ch}(1+\eta_{\rm ch})}J_{\rm ch} - \frac{(1-\eta_{\rm ch})}{(1+\eta_{\rm ch})}Q'_{\rm ch} \quad (9)$$

will in general deviate from the true radiance $I_{\rm ch}$. We define the error in the radiance that is derived from signal $J_{\rm ch}$ as

$$\epsilon_{\rm ch} = \frac{I'_{\rm ch}-I_{\rm ch}}{I_{\rm ch}}. \quad (10)$$

The simplest way of deriving radiances from observations by polarization sensitive instruments is to ignore the state of polarization of the observed light, thus to chose $Q'_{\rm ch} = 0$ in equation (9). In that case,

$$\epsilon_{\rm ch} = \frac{(1-\eta_{\rm ch})}{(1+\eta_{\rm ch})}\frac{Q_{\rm ch}}{I_{\rm ch}} = \frac{(\eta_{\rm ch}-1)}{(\eta_{\rm ch}+1)}P_{\rm ch}, \quad (11)$$

with $P_{\rm ch}$ the true degree of linear polarization of the observed light.

Regarding the GOME instrument, it is not necessary to completely ignore the polarized nature of the light reflected by Earth. In addition to the radiance channels, to which equation (7) applies, GOME has been equipped with special channels, the polarization measuring devices. The PMDs have been designed such that they are only sensitive to light that is polarized parallel to the slit of the GOME instrument. The signal measured by a PMD can thus be written as (cf. equation (7))

$$J_{\rm PMD} = \frac{1}{2}a_{\rm PMD}\,[I_{\rm PMD}+Q_{\rm PMD}], \quad (12)$$

with $a_{\rm PMD}$ the PMD's response to the parallel polarized light. Were the spectral response functions of the PMDs equal to those of the radiance channels, then $I_{\rm ch}$ and $Q_{\rm ch}$ would be equal to $I_{\rm PMD}$ and $Q_{\rm PMD}$, respectively, and $I_{\rm ch}$ could be derived from the combination of equations (7) and (12). Unfortunately, there are only three PMDs for GOME's 1024 radiance channels; they cover the wavelength regions from 300 to 400, 400 to 600, and 600 to 800 nm. Owing to the difference in spectral resolution, the broadband PMD measurements cannot be used directly to derive $I_{\rm ch}$. The steps involved in deriving $I_{\rm ch}$ from $J_{\rm ch}$ and $J_{\rm PMD}$ as measured by GOME are described in a so-called polarization correction algorithm [*Deutsche Forschungsanstalt für Luft- und Raumfahrt (DLR),* 1995]. The first step in this algorithm is the integration of the signals $J_{\rm ch}$ across the wavelength regions covered by the PMDs. With these integrated signals and the PMD measurements, a broadband value for the degree of polarization can be derived for each of the three wavelength regions. Considering the wavelength region containing the O_2 A band, which is covered by the third PMD, this broadband value of the degree of polarization $I_{\rm ch}$ is then used to derive $I_{\rm ch}$ from $J_{\rm ch}$.

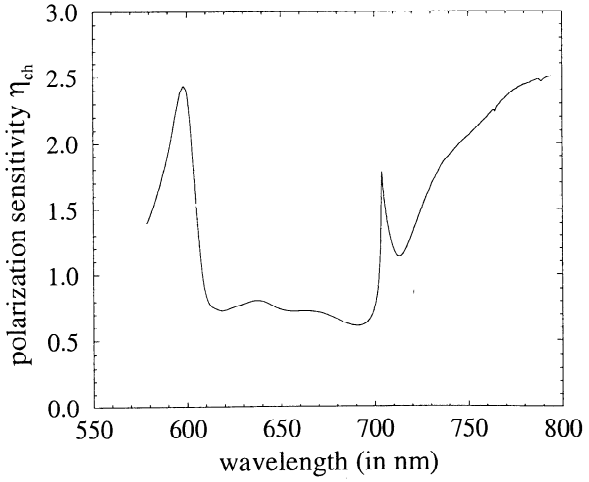

Figure 1. Polarization sensitivity $\eta_{\rm ch}$ of the GOME channels between 580 and 800 nm, as measured during the preflight calibration of the instrument [*TNO-TPD,* 1994]. In this wavelength region, GOME's polarization sensitivity is mainly due to the dispersion grating and dichroic mirror. Note that $\eta_{\rm ch} \approx 2$ in the wavelength region containing the O_2 A band.

The polarization is thus assumed to be constant across the O_2 A absorption band. Since this assumption is not generally valid, radiance errors in the band still occur. In this case, the error in the radiance derived from a signal J_{ch} is

$$\epsilon_{ch} = \frac{(1-\eta_{ch})}{(1+\eta_{ch})}\frac{(Q_{ch}-Q'_{ch})}{I_{ch}} = \frac{(\eta_{ch}-1)}{(\eta_{ch}+1)}(P_{ch}-P'_{ch}). \quad (13)$$

Here we write $P'_{ch} = -Q'_{ch}/I_{ch}$ for the broadband value of the degree of polarization. Model simulations show that for the O_2 A band wavelength region, the degree of linear polarization in the continuum outside the absorption band, P_{cont}, is a good approximation for the broadband value of the degree of polarization, P'_{ch}.

In this paper, we investigate radiance errors ϵ_{ch} both for the case in which the state of polarization of the observed light is ignored ($P'_{ch} = Q'_{ch} = 0$) and for the case in which a correction scheme as described above is applied, and the degree of polarization in the continuum is assumed to hold throughout the absorption band ($P'_{ch} = P_{cont}$).

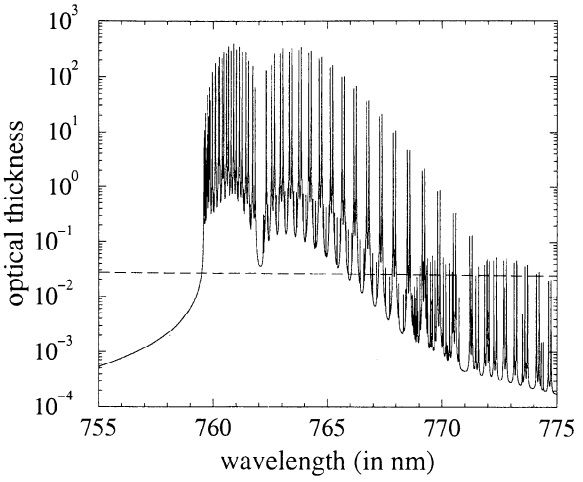

Figure 2. Molecular scattering optical thickness (dashed line) and the molecular absorption optical thickness (solid line) of the model atmosphere as a function of wavelength between 755 and 775 nm. Absorption line parameters have been taken from *Rothman et al.* [1992].

3. Simulating Observations

3.1. The Model Atmosphere

For our radiative transfer calculations, the terrestrial atmosphere is represented by a stack of 32 plane-parallel, homogeneous layers containing scattering and absorbing molecules. A plane-parallel homogeneous cloud is modeled by adding homogeneous, spherical, liquid water droplets to one or more atmospheric layers. The atmosphere is bounded below by a Lambertian reflecting surface. To calculate Stokes parameters of scattered sunlight emerging from the top of the model atmosphere, we have to specify the surface albedo and, for each atmospheric layer, the molecular scattering and absorption optical thicknesses. In the case in which an atmospheric layer contains a cloud, the cloud optical thickness as well as the scattering matrix and the single-scattering albedo of the cloud droplets have to be specified.

The altitude, ambient pressure, and temperature of the 33 levels bounding the layers of our model atmosphere have been chosen according to a midlatitude summer profile [*McClatchey et al.*, 1972]. Because O_2 is well mixed up to an altitude of at least 90 km, we assume its volume mixing ratio to be constant with altitude, namely, 0.209476 [*McClatchey et al.*, 1972]. Values for the absorption cross sections of O_2 in the A band have been taken from *Rothman et al.* [1992], and for individual absorption lines a Voigt profile has been assumed.

The molecular scattering and absorption optical thicknesses of the model atmosphere for the wavelength region containing the O_2 A band are shown in Figure 2. These atmospheric optical thicknesses are the sums of the respective optical thicknesses of the individual atmospheric layers, which have been calculated as described by *Stam et al.* [1999]. As can be seen in Figure 2, the molecular scattering optical thickness of the model atmosphere is almost constant across this wavelength region (and equal to 0.026 in the middle of the O_2 A band), whereas the molecular absorption optical thickness varies strongly with wavelength. Henceforth we will use the symbol b^m when referring to the atmospheric molecular absorption optical thickness.

The refractive index of the cloud droplets is taken from *Hale and Querry* [1973] and is 1.33 at 765 nm. For the size distribution of the droplets, a two-parameter gamma distribution has been chosen, which is given by [*Hansen and Travis*, 1974]

$$n(r) = Cr^{(1-3v_{eff})/v_{eff}} \exp\left[-r/(v_{eff}r_{eff})\right]. \quad (14)$$

Here $n(r)dr$ is the number of particles per unit volume with radii between r and $r + dr$, and C is a constant such that the total number of particles per unit volume equals 1. The effective radius r_{eff} of the cloud droplets is chosen to be equal to 10 μm, and the effective variance v_{eff} is 0.15.

For a given wavelength, the scattering properties of the cloud droplets are calculated by using Mie theory [*Van de Hulst*, 1957; *De Rooij and Van der Stap*, 1984]. In Figure 3, the phase function and the degree of linear polarization of light singly scattered by molecules, and the cloud droplets are shown as functions of the scattering angle Θ. Each phase function has been normalized such that its average over all directions is unity. The curves in Figure 3 are valid for light with $\lambda = 765$ nm, in the middle of the O_2 A band. Molecular scattering is calculated by taking into account a depolarization factor [*Hansen and Travis*, 1974] equal to 0.0277 at $\lambda = 765$ nm [*Bates*, 1984].

The standard model atmosphere that we use in our simulations is shown schematically in Figure 4. It con-

tains molecules up to an altitude of 100 km and a cloud in the atmospheric layer between 2 and 3 km; the underlying surface is black. The cloud has an optical thickness b^c of 16.0 at $\lambda = 550$ nm. Its optical thickness at another wavelength is obtained by multiplying b^c at 550 nm with the ratio of the cloud droplets' extinction cross section at the other wavelength to that at 550 nm. In particular, at $\lambda = 765$ nm, this ratio is 1.0113, and the cloud's optical thickness at 765 nm is thus 16.2.

Our standard model atmosphere contains no aerosol particles. In the discussion (section 5), we address the influence of aerosol particles on the simulated observations and the errors as presented in section 4. We will also discuss the influence of a reflecting surface.

3.2. Radiative Transfer Calculations

For a given model atmosphere-surface system, we calculate the Stokes parameters of scattered light emerging from the top of the atmosphere by using an adding-doubling algorithm [*Van de Hulst,* 1980], which fully includes multiple scattering and polarization [*Hansen,* 1971; *Hovenier,* 1971; *De Haan et al.,* 1987]. With these Stokes parameters, we simulate I_{ch}, P_{ch}, and the errors ϵ_{ch} in radiances derived from simulated observations.

The incoming sunlight is assumed to be unpolarized and unidirectional, with an irradiance πF_0, measured perpendicularly to the direction of incidence. The solar zenith angle is denoted by θ_0. We present reflectivities $R_{ch} = I_{ch}/\cos\theta_0 F_0$, rather than reflected radiances.

We limit our calculations to reflected light coming from the nadir direction. We choose this geometry not only because it corresponds to an often used viewing direction for satellite instruments, for example, for GOME and SCIAMACHY, but also because it does not depend on the azimuthal angle and therefore shortens the computing time. The latter is very important in time-consuming radiative transfer calculations including polarization and clouds.

3.2.1. High-spectral resolution. The results for the Dirac delta function shaped response function will be presented in section 4.1, as functions of the atmospheric absorption optical thickness b^m instead of as functions of the wavelength. As can be seen in Figure 2, b^m varies approximately between about 10^{-3} and $2\cdot10^2$ between 755 and 775 nm. These values of b^m have been calculated by taking the (wavelength dependent) temperature and pressure dependence of the absorption cross sections fully into account [see *Stam et al.*, 1999]. For our radiative transfer calculations, we vary b^m from 10^{-3} to $2\cdot10^2$, assuming that the absorption cross section decreases linearly with altitude in the atmosphere, such that at 100 km, the cross section is 10^{-8} times that at the surface. Details on this approach to calculate the molecular absorption optical thickness of atmosphere can be found in the work ofthe work of *Stam et al.* [1999]. We use the scattering properties of the molecules and the cloud droplets at $\lambda = 765$ nm for the entire interval of the O_2 A band.

3.2.2. GOME spectral resolution. GOME's spectral response function covers a large number of individual absorption lines in the O_2 A band wavelength region. Consequently, monochromatic, line-by-line radiative transfer calculations, including polarization for

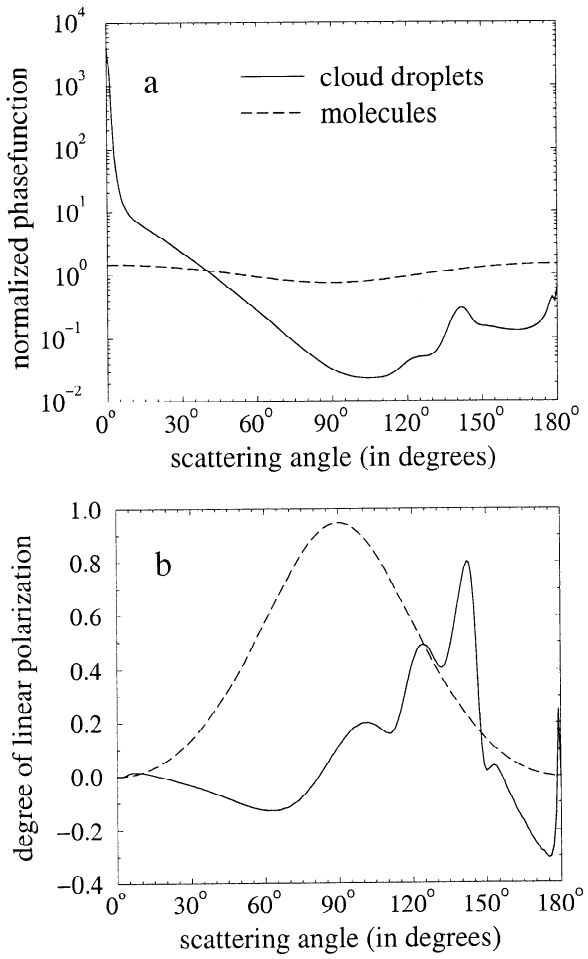

Figure 3. (a) Phase function and (b) degree of linear polarization P_s as functions of the scattering angle for light singly scattered by cloud droplets (solid line) and molecules (dashed line). The wavelength of the light is 765 nm.

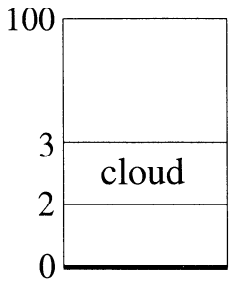

Figure 4. Schematic representation of the standard model atmosphere. The 32 layers with molecules, in which the atmosphere has been divided, are not shown, except for the layer which contains the cloud with $b^c = 16.0$. Altitudes are given in kilometers.

a model atmosphere with clouds, would require an enormous amount of computing time. Therefore we calculate the Stokes parameters of scattered sunlight emerging from the top of the atmosphere by using the correlated k distribution method (the ck method) (see, e.g., *Lacis and Oinas* [1991]), extended to include an instrumental spectral response function [*Stam et al.*, 2000].

The ck method is an approximate method; hence the calculated radiances and degree of polarization can deviate from those obtained by using line-by-line calculations. We have calculated these errors by comparing results obtained by using the ck method with results obtained by using line-by-line calculations for the standard model atmosphere-surface system and for the spectral channel around $\lambda_{ch} = 760.6$ nm. In this spectral channel, which covers the wavelength region with the strongest absorption lines (see Figure 2), we expect the errors in both the radiance and the degree of linear polarization due to the assumptions made in the ck method to be the largest [*Stam et al.*, 2000]. Defining the error in the radiances calculated by using the ck method as $(I_{ch}^{ck} - I_{ch}^{lbl})/I_{ch}^{lbl}$ and the error in the degree of linear polarization as $P_{ch}^{ck} - P_{ch}^{lbl}$, we found errors up to 6% for the radiances and up to 0.001 for the polarization. These results are based on a few sample calculations. In view of the large computational effort required for these comparisons, we did not further investigate the errors of the ck method for cloudy atmospheres. Since it is the degree of linear polarization that is needed to calculate the radiance error due to using polarization sensitive instruments (see equations (11) and (13)), the ck method appears to be accurate enough for our purposes.

4. Numerical Results

4.1. High Spectral Resolution

4.1.1. Standard model atmosphere. The standard model atmosphere contains a cloud with an optical thickness b^c equal to 16.0 (at 550 nm), with its bottom at an altitude of 2 km and its top at 3 km. Figure 5 shows the reflectivity R_{ch} and the degree of linear polarization P_{ch} of light emerging from the top of the model atmosphere as functions of the atmospheric molecular absorption optical thickness b^m. The reflected light comes from the nadir direction, and three values for the solar zenith angle θ_0 are considered: 20°, 40°, and 60°. The curves suggest a distinction in three regions of b^m: namely, $b^m \ll 1$, $b^m \gg 1$, and a transition region in between. Comparison with Figure 2 shows that the first region mainly applies to the continuum and the weak absorption lines, whereas the second region represents the strongest absorption lines. In the following, we will discuss the scattering processes that determine the shape of the curves in Figure 5 in the regions distinguished above.

At wavelengths in and near the O_2 A band, the molecular scattering optical thickness of our model atmosphere is only 0.026 (see Figure 2). Thus in the region where $b^m \ll 1$ in Figure 5, R_{ch} and P_{ch} are predominantly determined by light that has been scattered by the cloud particles. This explains the similarity between the scattering angle dependence of the phase function and the degree of linear polarization of the cloud droplets as shown in Figure 3 and the solar zenith dependence of the curves in Figure 5 in this region. In particular for $\theta_0 = 40°$, the relatively large values of R_{ch} and P_{ch} in Figure 5 can be attributed to the local maxima in the phase function and the degree of linear polarization around the scattering angle $\Theta = 142°$, respectively, in Figure 3. These maxima are associated with the primary rainbow. Owing to multiple scattering within the cloud, the absolute value of P_{ch} in Figure 5b is much smaller than the corresponding single-scattering value shown in Figure 3b.

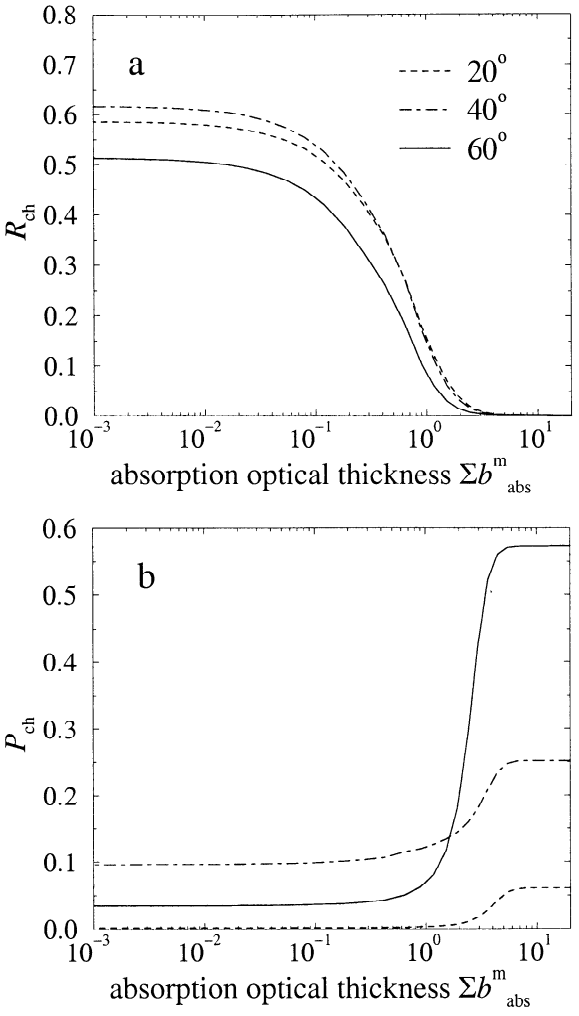

Figure 5. High spectral resolution: (a) reflectivity R_{ch} and (b) degree of linear polarization P_{ch} of light reflected perpendicularly upward by the standard model atmosphere as a function of the atmospheric molecular absorption optical thickness b^m. The light comes from the nadir direction, and the following values of the solar zenith angle θ_0 are employed: 20° (dashed line), 40° (dot-dashed line), and 60° (solid line).

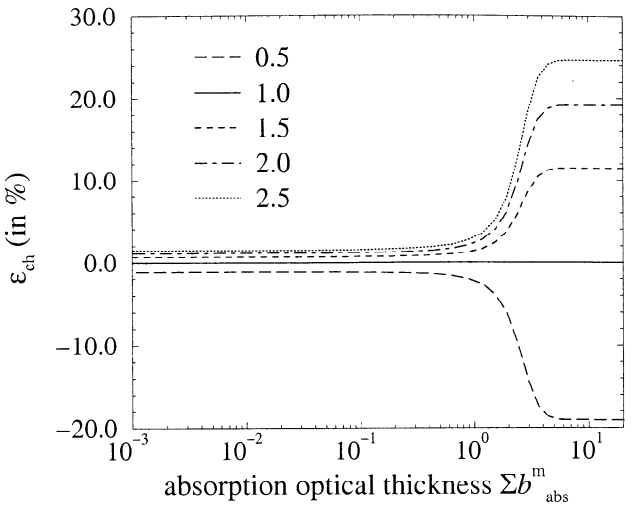

Figure 6. High spectral resolution: error ϵ_{ch} in the derived radiance I'_{ch} of light reflected perpendicularly upward by the standard model atmosphere as a function of b^m for $\theta_0 = 60°$ and $P'_{ch} = 0$. The following values of η_{ch} are employed: 0.5 (long-dashed line), 1.0 (solid line), 1.5 (short-dashed line), 2.0 (dot-dashed line), and 2.5 (dotted line).

At values of $b^m \gg 1$, R_{ch} and P_{ch} in Figure 5 approach the respective values that are found in the strongest absorption lines of the O_2 A band. With such large absorption optical thicknesses, the fraction of incoming sunlight that reaches the cloud layer is very small, and the fraction of light that is scattered upward by the cloud droplets and emerges from the top of the atmosphere is practically negligible. Therefore R_{ch} is very small, and P_{ch} is predominantly determined by molecular scattering in the atmospheric layers above the cloud. Since multiple scattering is suppressed by the strong absorption, P_{ch} depends mainly on single scattering. Therefore the maximum values of P_{ch} in Figure 5b equal the single-scattering degree of polarization for molecules in Figure 3b at the corresponding scattering angles.

Figure 6 shows the errors ϵ_{ch} in the derived radiances I'_{ch} for the case $\theta_0 = 60°$ and for values of the instrumental polarization sensitivity η_{ch} that are typical for GOME (see Figure 1). The errors have been calculated by using equation (11) (thus $P'_{ch} = 0$). Clearly (see also equation (11)), for $\eta_{ch} < 1.0$, the derived radiance I'_{ch} is smaller than the true radiance I_{ch} for all values of b^m, whereas for $\eta_{ch} > 1.0$, it is larger. Furthermore, it can be seen that for a given value of η_{ch} unequal to 1.0, the absolute value of ϵ_{ch} increases with b^m. Thus the errors are largest in the strongest absorption lines. Since in the continuum the derived radiance deviates less from the true radiance than in the absorption lines, the shape of the derived radiance spectrum deviates from the true shape. For example, when $\eta_{ch} > 1.0$, the absorption lines in the derived radiance spectrum will be less deep (measured with respect to the continuum) than in the true spectrum.

The curves in Figure 6 have been obtained by using $P'_{ch} = 0$. When the degree of polarization in the continuum is known and $P'_{ch} = P_{cont}$, ϵ_{ch} will decrease for all values of b^m with an amount that makes ϵ_{ch} vanish at the smallest values of b^m, as is obvious from equation (13). For example, with $\eta_{ch} = 2$, ϵ_{ch} would then be zero in the continuum but still about 18% in the strongest absorption lines.

In Figure 7, R_{ch} and P_{ch} of light from the nadir direction are shown as functions of the solar zenith angle θ_0 for three values of b^m, namely, 0.001, 1.0, and 10.0 (in the latter case, R_{ch} is virtually zero). The local maxima around $\theta_0 = 40°$ both in R_{ch} and P_{ch} for $b^m = 0.001$ and 1.0 correspond with the primary rainbow maxima in the single-scattering phase function and degree of linear polarization of cloud droplets (see Figure 3). The negative values of P_{ch} in Figure 7b for θ_0 smaller than about 20° are attributed to the negative values of the degree of polarization for the cloud droplets that occur for scattering angles Θ between about 150° and 180°

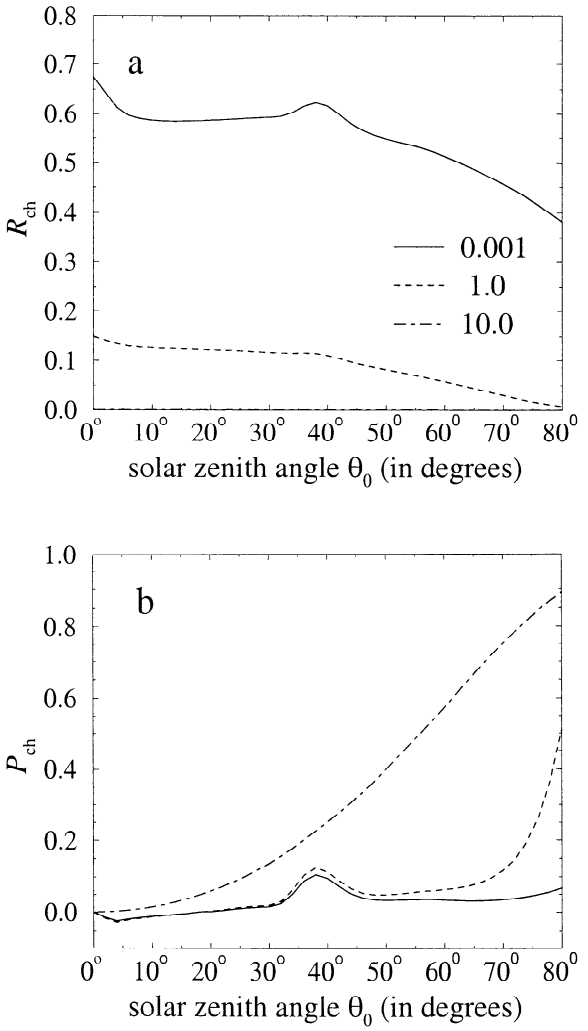

Figure 7. High spectral resolution: (a) R_{ch} and (b) P_{ch} of light reflected perpendicularly upward by the standard model atmosphere as a function of the solar zenith angle θ_0 for $b^m = 0.001$ (solid line), 1.0 (dashed line), and 10.0 (dot-dashed line).

in Figure 3b. The solar zenith angle dependence of P_{ch} for $b^m = 10.0$ corresponds to the scattering angle dependence of the degree of polarization for single scattering by molecules (see Figure 3b). From Figure 7b it can be concluded that since P_{ch} of the reflected light depends strongly on θ_0 so does the error ϵ_{ch}, regardless of whether $P'_{ch} = 0$ or $P'_{ch} = P_{cont}$.

4.1.2. Influence of cloud top altitude. The curves in Figure 8 show the influence of the cloud top altitude on R_{ch} and P_{ch} of light from the nadir direction for $\theta_0 = 60°$. The cloud, with $b^c = 16.0$ (at 550 nm) and with a geometrical thickness of 1 km, is placed with its top at altitudes of 2, 3, or 4 km.

As can be seen in Figure 8, both at the smallest and at the largest values of b^m, the altitude of the cloud top hardly influences R_{ch} or P_{ch}. For $b^m \ll 1$, this is due to the small scattering optical thickness of the atmosphere above the cloud: compared with the light scattered by the cloud particles, the light scattered by the molecules above the cloud is practically negligible for the three cloud top altitudes. For $b^m \gg 1$, only light that has been scattered in the highest, cloudless, atmospheric layers can emerge from the top of the atmosphere, so that variation in the cloud top altitude has no effect. For intermediate absorption optical thicknesses, say between 0.01 and 5, an increase of the cloud top altitude results in an increase in radiances due to the decreasing amount of absorbing molecules above the cloud, and a decrease of the degree of linear polarization, due to the decrease of molecular scattering above the cloud.

From the curves in Figure 8b, it can be concluded that the cloud top altitude hardly influences the error ϵ_{ch} in the derived radiances in the continuum outside the O_2 A band and in the strongest absorption bands. At wavelengths where the absorption optical thickness

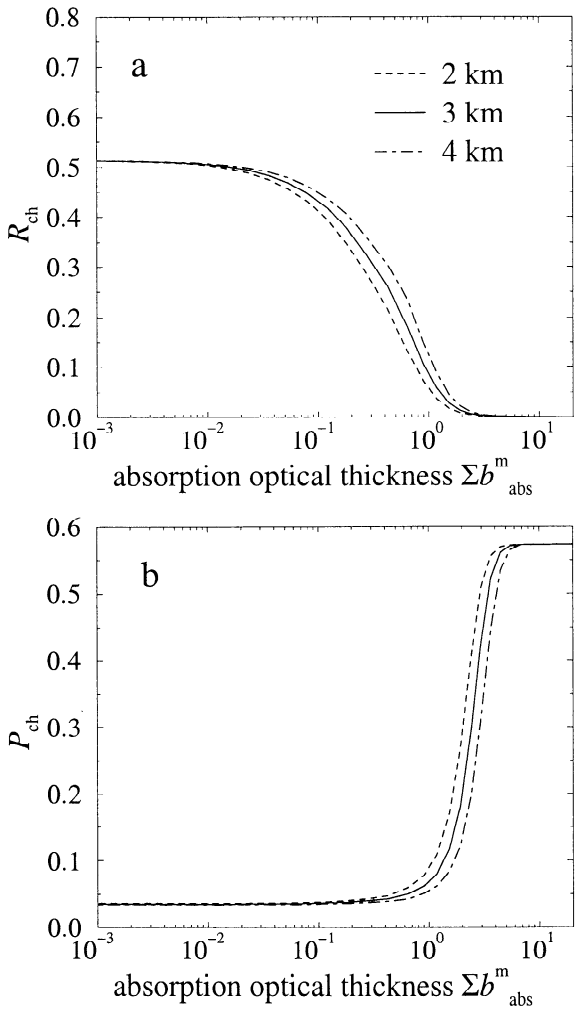

Figure 8. High spectral resolution: (a) R_{ch} and (b) P_{ch} of light reflected perpendicularly upward by a model atmosphere containing a cloud with $b^c = 16.0$ and a geometrical thickness of 1 km, as a function of b^m. Solar zenith angle $\theta_0 = 60°$, and the following cloud top altitudes are employed: 2 km (dashed line), 3 km (solid line), and 4 km (dot-dashed line).

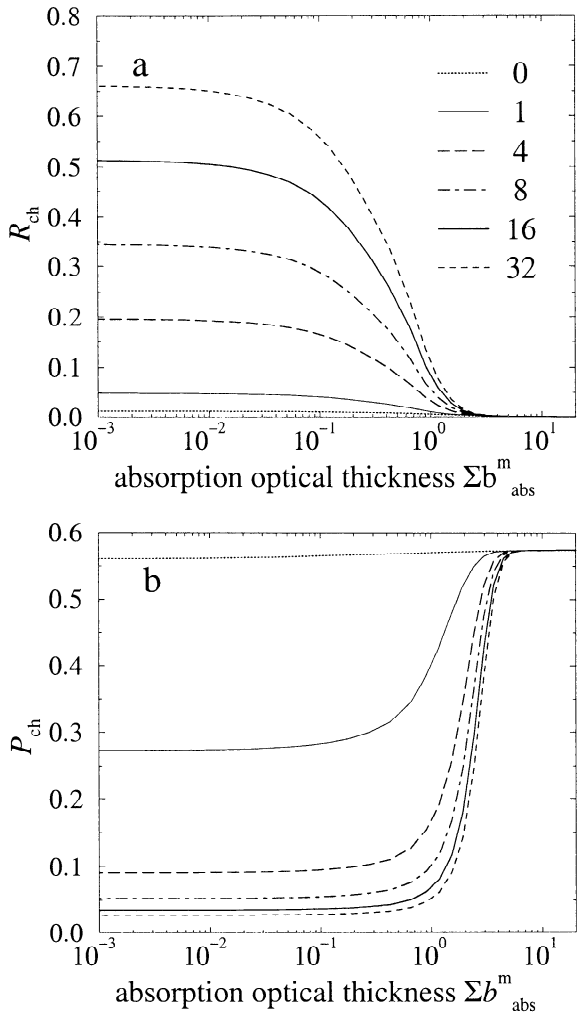

Figure 9. High spectral resolution: (a) R_{ch} and (b) P_{ch} of light reflected perpendicularly upward by a model atmosphere containing a cloud with a geometrical thickness of 1 km and with its top at 3 km, as a function of b^m. Solar zenith angle $\theta_0 = 60°$. The following values of the cloud optical thickness b^c are employed: 0.0 (dotted line), 1.0 (thin solid line), 4.0 (long-dashed line), 8.0 (dot-dashed line), 16.0 (thick solid line), and 32.0 (short-dashed line).

is between about 0.01 and 5, however, the difference between the derived and the true radiance increases with decreasing cloud top altitude, for any η_{ch}.

4.1.3. Influence of cloud optical thickness. In the standard model atmosphere, the cloud optical thickness b^c is 16.0 (at 550 nm). The influence of b^c on R_{ch} and P_{ch} of light from the nadir direction can be inferred from Figure 9, where curves are shown for b^c ranging from 0.0 to 32.0 (at 550 nm). The cloud extends from 2 to 3 km. The solar zenith angle $\theta_0 = 60°$.

When $b^c = 0.0$, the model atmosphere contains only molecules. In this extreme case, the reflected radiance is small for all values of b^m, because the scattering optical thickness of the molecules is small and because the surface below our standard model atmosphere is black. The degree of linear polarization of this light is high for all values of b^m, because for this geometry the light singly scattered by molecules is strongly polarized (see Figure 3, at $\Theta = 120°$) and because the contribution of multiply scattered light, with in general a low degree of polarization, is small. The slight increase of P_{ch} with b^m that can be seen in Figure 9b is due to the decrease of the small contribution of multiple scattering with increasing molecular absorption in the atmosphere [*Stam et al.*, 1999].

With increasing cloud optical thickness, we see that for values of b^m smaller than about 5, R_{ch} increases, whereas P_{ch} decreases. For b^m larger than about 5, the cloud is not observable in the reflectivity or in the polarization, i.e. the results coincide with those for the cloudless molecular atmosphere.

From the curves in Figure 9b it can be seen that except for $b^m \gg 1$, P_{ch} depends strongly on the cloud optical thickness b^c. Thus when radiances are derived from observations under the assumption that the reflected light is unpolarized ($P'_{ch} = 0$), the error ϵ_{ch} will depend on b^c, except in the strongest absorption lines. In the case $P'_{ch} = P_{cont}$ is known, the errors at the smallest values of b^m vanish, and those in the strongest absorption lines are reduced. In Table 1, typical values of ϵ_{ch} can be found for $\eta_{ch} = 2$ and b^c equal to 0.0, 1.0, and 16.0 for $b^m = 0.001$, which is representative for the continuum, and for $b^m = 10$, which represents the strongest absorption lines. Clearly, in the case in which it is assumed that the observed light is unpolarized (thus $P'_{ch} = 0$), the errors in the derived radiances are larger than those for the case $P'_{ch} = P_{cont}$. The advantage of knowing P_{cont} is apparently largest for small cloud optical thicknesses, at least for a black surface as considered here.

Table 1. Error ϵ_{ch} (in Percent) in Radiance Derived From Observations of an Instrument With a Delta-Function-Shaped Response Function and With $\eta_{ch} = 2.0$ for Three Values of Cloud Optical Thickness b^c (at 550 nm) for Light From the Nadir Direction and for $\theta_0 = 60°$

	$b^m = 0.001$		$b^m = 10.0$	
b^c	$P'_{ch} = 0$	$P'_{ch} = P_{cont}$	$P'_{ch} = 0$	$P'_{ch} = P_{cont}$
0.0	18.7	0.0	19.1	0.4
1.0	9.1	0.0	19.1	10.0
16.0	1.2	0.0	19.1	18.0

Errors are given for $b^m = 0.001$ (the continuum) and for $b^m = 10.0$ (the strongest absorption lines). $P'_{ch} = 0$ pertains to the case in which the observed light is assumed to be unpolarized (see equation (11)), and $P'_{ch} = P_{cont}$, to the case in which the continuum degree of linear polarization is adopted (see equation (13)).

4.2. GOME Spectral Resolution

4.2.1. Standard model atmosphere. Henceforth, we will employ the Gaussian-shaped instrumental spectral response function that is representative for GOME (see equation (5)). Figure 10 shows the reflectivity R_{ch} and the degree of linear polarization P_{ch} of light reflected perpendicularly upwards by the standard model atmosphere for the wavelengths λ_{ch} of the instrumental channels. The curves in Figure 10 have been calculated for the same solar zenith angles as those in Figure 5, namely, 20°, 40°, and 60°.

In the channels near $\lambda = 755$ nm and 775 nm, the atmospheric absorption optical thickness b^m is smaller than 0.01 (see Figure 2). Therefore for a given solar zenith angle, R_{ch} and P_{ch} calculated for these channels as shown in Figure 10, are equal to R_{ch} and P_{ch} at the smallest values of b^m in Figure 5.

The channels near $\lambda = 761$ nm cover wavelength regions with the largest average values of b^m that can be found in the O_2 A band (see Figure 2). Since the spectral response function of GOME is broad in comparison with the Dirac delta function, it generally comprises wavelength regions with large values of b^m, as well as regions with small values of b^m. Therefore the minimum (maximum) value attained by R_{ch} (P_{ch}) in Figure 10 is larger (smaller) than that in Figure 5 for the same solar zenith angle.

Figure 11 shows the error ϵ_{ch} in the derived radiance I'_{ch} for $\theta_0 = 60°$ for values of η_{ch} ranging from 0.5 to 2.5 and with $P'_{ch} = 0.0$. Comparison with ϵ_{ch} for $b^m \ll 1$ in Figure 6 reveals that application of the Gaussian-shaped spectral response function, instead of a delta-function-shaped one, hardly influences the errors in the continuum. Inside the O_2 A band, however, the errors decrease significantly when the Gaussian function instead of the delta function is applied. For example, for $\eta_{ch} = 2.0$ (which is a representative value for GOME in the O_2 A band), the largest value of ϵ_{ch} is about 19% in Figure 6, whereas it is only about 2.3% in Figure 11. When $P'_{ch} = P_{cont}$ is used, like in the case of GOME, the errors as shown in Figure 11 vanish in the continuum, and they decrease at other wavelengths λ_{ch} such that, for example, for $\eta_{ch} = 2.0$ the maximum radiance error will be 1.2% (taking $P'_{ch} = 0.035$).

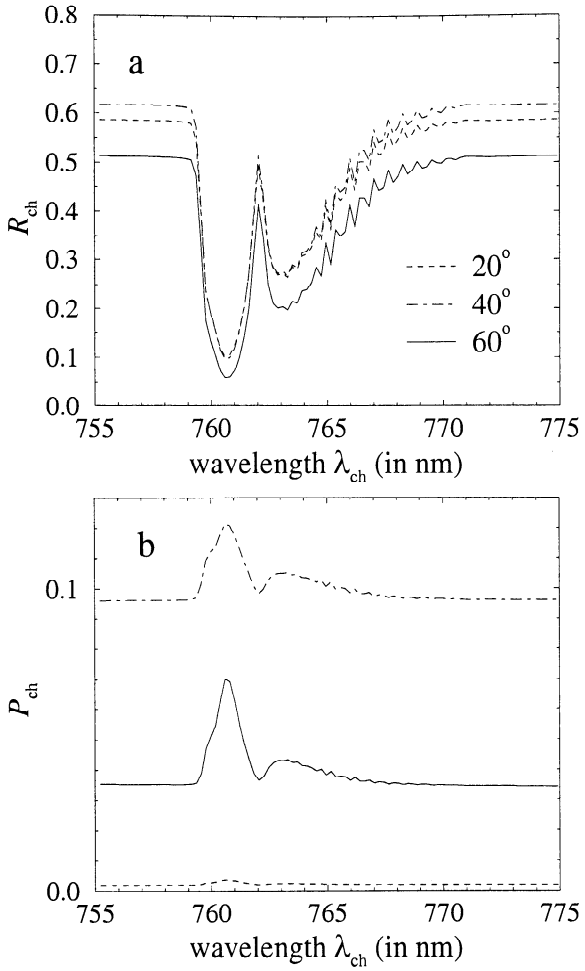

Figure 10. GOME spectral resolution: (a) R_{ch} and (b) P_{ch} of light reflected perpendicularly upward by the standard model atmosphere as a function of the wavelength λ_{ch}. The following values of θ_0 are employed: 20° (dashed line), 40° (dot-dashed line), and 60° (solid line).

Because the radiance errors in the continuum in general differ from the errors in the absorption band, the shape of the band as derived from the observations will in general deviate from the true shape of the band. In particular, when $\eta_{ch} > 1.0$, the derived radiance in the absorption band is larger than the true radiance.

4.2.2. Influence of cloud top altitude. To illustrate the influence of the cloud top altitude on R_{ch} and P_{ch}, we consider a channel measuring outside the O_2 A band, with $\lambda_{ch} = 755.2$ nm, and the channel with $\lambda_{ch} = 760.6$ nm, which covers the wavelength region with some of the strongest absorption lines. For these two channels, the curves in Figure 12 show the reflectivity and the degree of linear polarization of light from the nadir as a function of the cloud top altitude. The cloud optical thickness is 16.0, and its geometrical thickness is 1 km. The solar zenith angle is 60°, which facilitates comparison with Figure 8.

Figure 12a clearly shows that the radiance in the channel measuring in the continuum (with $\lambda_{ch} = 755.2$ nm) is insensitive to changes in the altitude of the top of our model cloud. This was also apparent in Figure 8. The degree of linear polarization (Figure 12b) in the continuum is only slightly sensitive to the cloud top altitude: P_{ch} decreases with about 0.003 with an increase of the cloud top altitude with 2 km. Regarding the channel inside the O_2 A band (with $\lambda_{ch} = 760.6$ nm), both R_{ch} and P_{ch} depend significantly on the cloud top altitude: R_{ch} more than doubles and P_{ch} decreases more than 0.03 with a cloud top altitude's increase of 2 km.

From the curves in Figure 12 it can be deduced that when the cloud top altitude increases, the reflectivity inside the band increases and the degree of linear polarization decreases, making the O_2 A band less prominent in both the reflectivity and polarization. As was mentioned in section 1, the relation between the difference in reflectivity outside and inside the O_2 A absorption band, on the one hand, and the cloud top altitude, on the other hand, is being used to derive cloud top altitudes from satellite reflectivity measurements. As far as we know, no algorithm has yet been proposed to derive cloud top altitudes using the difference in the degree of linear polarization outside and inside the O_2 A band.

Since P_{ch} in the continuum outside the O_2 A band hardly depends on the cloud top altitude, the error in the derived radiance ϵ_{ch} in the continuum is also hardly cloud top altitude dependent. According to the curves in Figure 12, for $\eta_{ch} = 2.0$ and $P'_{ch} = 0.0$, ϵ_{ch} in the continuum is about 1.2%. At wavelengths inside the O_2 A band, the absolute error decreases with increasing cloud top altitude. For example, choosing $\eta_{ch} = 2.0$ and $P'_{ch} = 0.0$, ϵ_{ch} at 760.6 nm is 3% in the case the cloud top is at 2 km, and about 1.9% with the top at 4 km.

When, instead of zero, the continuum value P_{cont} is used for P'_{ch}, the radiance errors at 760.6 nm are 1.8%

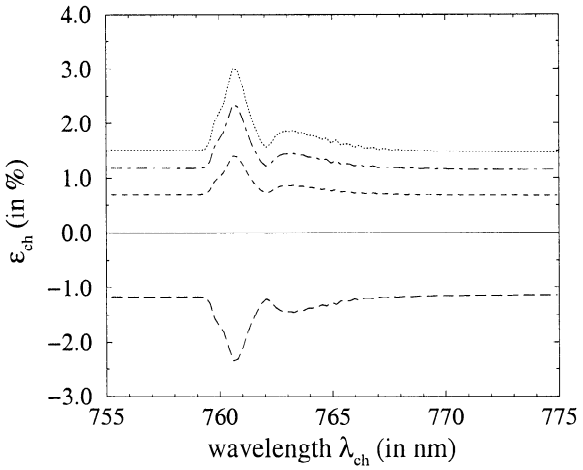

Figure 11. GOME spectral resolution: Error ϵ_{ch} in the derived radiance I'_{ch} of light reflected perpendicularly upward by the standard model atmosphere as a function of λ_{ch}. Solar zenith angle $\theta_0 = 60°$. Assuming $P'_{ch} = 0$, the following values of η_{ch} are employed: 0.5 (long-dashed line), 1.0 (solid line), 1.5 (short-dashed line), 2.0 (dot-dashed line), and 2.5 (dotted line).

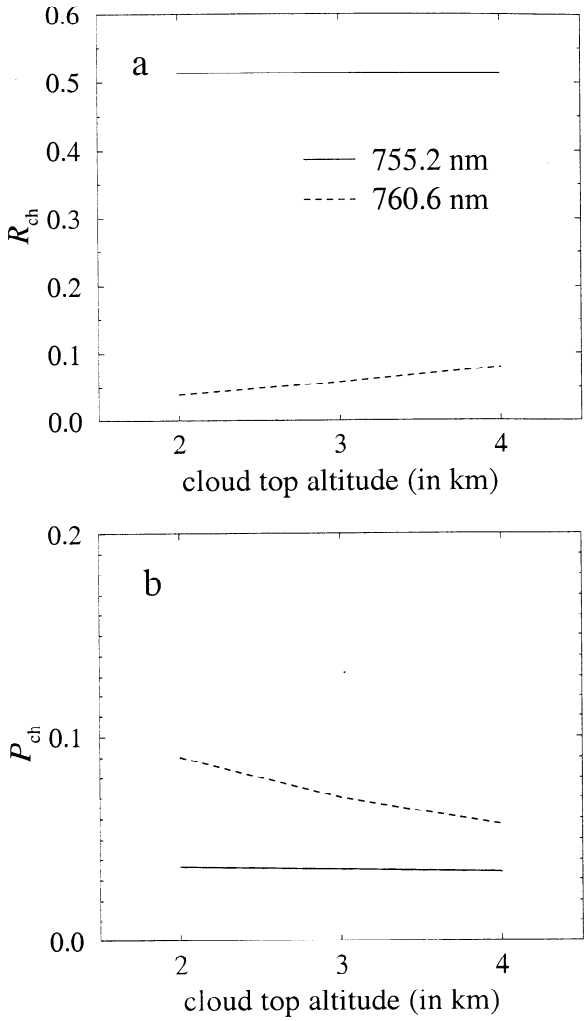

Figure 12. GOME spectral resolution: (a) R_{ch} and (b) P_{ch} of light reflected perpendicularly upward by a model atmosphere containing a cloud with $b^c = 16.0$ and a geometrical thickness of 1 km, as a function of the cloud top altitude. Solar zenith angle $\theta_0 = 60°$. The following values of λ_{ch} are employed: 755.2 nm (solid line) and 760.6 nm (dashed line).

for a cloud top at 2 km and 0.8% for a top at 4 km (assuming $\eta_{ch} = 2.0$). In this case the radiance error in the continuum vanishes. Hence the absorption band in the derived radiance spectrum will be slightly less deep with respect to the continuum than in the true spectrum.

4.2.3. Influence of cloud optical thickness. In Figure 13, R_{ch} and P_{ch} of light from the nadir direction in the channels with $\lambda_{ch} = 755.2$ nm and $\lambda_{ch} = 760.6$ nm are shown for various values of the cloud optical thickness b^c. The cloud is located in the atmospheric layer between 2 and 3 km, and $\theta_0 = 60°$.

In both channels, the radiance of the reflected light increases when the cloud optical thickness increases from 0.0 up to 32.0 (see Figure 13a). In the channel outside the O_2 A band (at 755.2 nm), the reflectivity at $b^c = 32.0$ is approximately 50 times that at $b^c = 0.0$, whereas inside the band (at 760.6 nm), the reflectivity increases by only a factor of 15, going from $b^c = 0.0$ to $b^c = 32.0$.

In both channels, P_{ch} decreases with increasing b^c (see Figure 13b). The difference between P_{ch} outside the band and P_{ch} inside the band is smallest when the atmosphere contains only molecules and no cloud ($b^c = 0.0$); it increases up to a difference of about 0.12 around $b^c = 1.5$ and then decreases again.

Because P_{ch} in the continuum depends on the cloud optical thickness, the error ϵ_{ch} in the continuum depends on b^c, too. Like P_{ch}, this error decreases with increasing cloud optical thickness. P_{ch} and the error in the continuum are not expected to vanish completely when b^c goes to infinity, since light scattered by the cloud particles is in general polarized, as can be seen in Figure 3b. For all values of b^c, the error at wavelengths

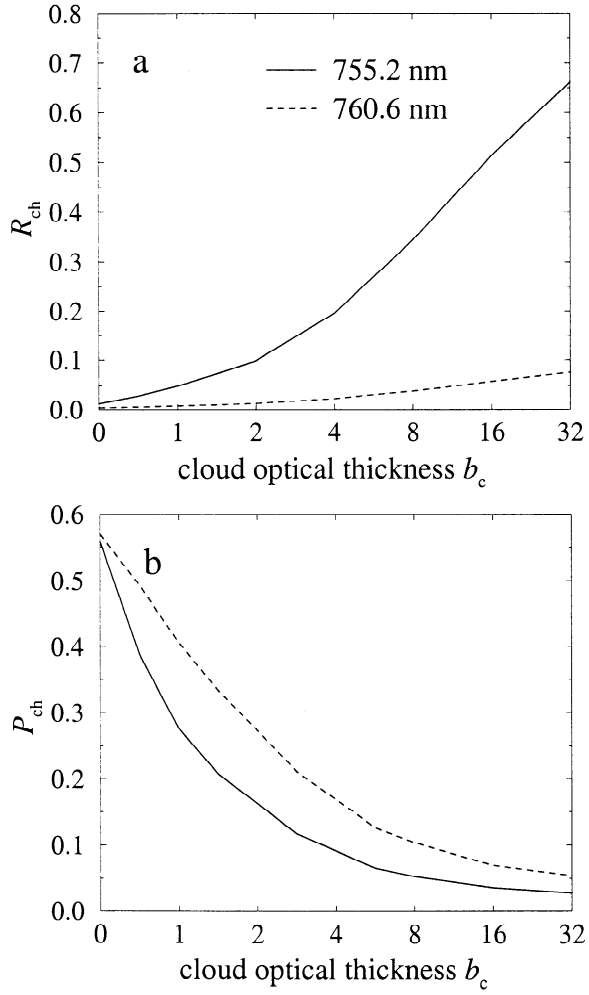

Figure 13. GOME spectral resolution: (a) R_{ch} and (b) P_{ch} of light reflected perpendicularly upward by a model atmosphere containing a cloud with a geometrical thickness of 1 km and a top altitude of 3 km, as a function of the cloud optical thickness b^c. Solar zenith angle $\theta_0 = 60°$. The following values of λ_{ch} are employed: 755.2 nm (solid line) and 760.6 nm (dashed line). The curves are not perfectly smooth owing to a limited number of calculations.

inside the O_2 A band will be larger than that in the continuum, because P_{ch} is larger inside the band than outside. Thus for all values of b^c, the shape of the band in the derived radiances deviates from the true shape.

In the case in which P_{ch} in the continuum is known, ϵ_{ch} in the continuum vanishes, and ϵ_{ch} at wavelengths inside the band decreases with respect to the values mentioned above. In this case, the radiance errors in the band are small for $b^c = 0.0$. They increase with increasing cloud optical thickness up to about 1.5, and they decrease again with increasing values of b^c.

Table 2 contains typical radiance errors for $\eta_{ch} = 2.0$, both in the continuum and inside the band, for b^c equal to 0.0, 1.0, and 16.0 and for a solar zenith angle θ_0 equal to 60°. Note that in particular for $b^c = 0.0$ and $P'_{ch} = P_{cont}$, the listed errors are small because in this case the model atmosphere contains only molecules, with a small scattering optical thickness, and because the surface is black. These errors are expected to increase upon adding aerosol to the model atmosphere or upon increasing the surface albedo (see section 5).

5. Discussion

The model atmosphere that was used in this paper was bounded below by a black surface, and it contained only gaseous molecules and cloud droplets. A more complicated, and more realistic, model atmosphere also contains aerosol particles and a natural surface which in general reflects part of the incident light (see, for example, *Bowker et al.* [1985]). We have performed some numerical simulations for such an atmosphere-surface model, and we summarize the results here.

Adding aerosol particles to a model atmosphere influences the reflected radiation in approximately the same manner as adding an optically thin cloud (with $b^c = 0.1 - 0.5$) to the atmosphere. Our simulations indeed show that the error in the derived radiance across the O_2 A absorption band for an aerosol-loaded atmosphere is about the same as the error obtained for an optically thin cloud. Further, an increase of the surface albedo changes the reflected radiation in approximately the same manner as an increase in the cloud optical thickness does, and the errors in the derived radiances are similar to those for a cloud-covered atmosphere. The solid curve in Figure 13a, which represents the reflectivity in the continuum outside the O_2 A band, can be used to crudely estimate the influence of a reflecting surface on the degree of polarization of the light reflected by a model atmosphere and thus on the radiance errors. That is, by taking the reflectivity R_{ch} to be the surface albedo, this curve gives a corresponding cloud optical thickness with approximately the same influence on the reflected radiation as a reflecting surface would have. With the curves in Figure 13b, one can subsequently derive the corresponding degree of linear polarization both inside and outside the band.

From the results presented in section 4, we conclude that in the O_2 A band, the errors in radiances derived from observations by polarization sensitive instruments in general increase with increasing spectral resolution (i.e., decreasing width of the instrumental spectral response function). On the other hand, the sensitivity of radiance observations to atmospheric parameters, such as cloud top height, appears to increase with increasing spectral resolution (see also, e.g., *Fischer and Grassl* [1991], *O'Brien and Mitchell* [1992], and *Nakajima et al.* [1998]). Obviously, to actually obtain more information by increasing the spectral resolution, it is important that the polarization sensitivity of the instrument is suppressed as much as possible.

For an instrument with a given polarization sensitivity, probably the best way to decrease errors in the radiances is by measuring the state of polarization of the observed light simultaneously with the radiances themselves. This approach has been chosen for the GOME and SCIAMACHY satellite instruments. However, the polarization measuring channels of these instruments have a low spectral resolution as compared with the spectral resolution of the channels intended to measure radiances. Consequently, radiance errors up to a few percent can still occur in spectral features such as the O_2 A band. Obviously, to significantly decrease radiance errors, the polarization should be measured with preferably the same spectral resolution as the radiances. Not only could such polarization measurements be used to minimize the radiance errors due to the instrumental polarization sensitivity, the state of polarization of the observed light could also provide additional information on the atmospheric constituents (see, e.g., *Mishchenko and Travis* [1997] and references therein).

Table 2. Same as Table 1 (Error ϵ_{ch} in Percent) Except for GOME Spectral Resolution

	$\lambda_{ch} = 755.2$ nm		$\lambda_{ch} = 760.6$ nm	
b^c	$P'_{ch} = 0$	$P'_{ch} = P_{cont}$	$P'_{ch} = 0$	$P'_{ch} = P_{cont}$
0.0	18.7	0.0	19.0	0.3
1.0	9.2	0.0	13.5	4.3
16.0	1.2	0.0	2.3	1.2

Errors are given for $\lambda_{ch} = 755.2$ nm (the continuum) and for $\lambda_{ch} = 760.6$ nm (deepest part of the absorption band).

Acknowledgments. This research has been supported by the Netherlands Organization for Scientific Research through Space Research Organization Netherlands.

References

Aben, I., F. Helderman, D. M. Stam, and P. Stammes, Spectral fine-structure in the polarization of skylight, *Geophys. Res. Lett.*, *26*, 591–594, 1999.

Bates, D. R., Rayleigh scattering by air, *Planet. Space Sci.*, *32*, 785–790, 1984.

Bowker, D. E., R. E. Davis, D. L. Myrick, K. Stacy, and W. T. Jones, Spectral reflectances of natural targets for use in remote sensing studies, *NASA RP-1139*, 181 pp., 1985.

Burrows, J. P., et al., SCIAMACHY - A European proposal for atmospheric remote sensing from the ESA Polar platform, Max-Planck-Institut für Chemie, Mainz, Germany, 1988.

Burrows, J. P., et al., The Global Ozone Monitoring Experiment (GOME): Mission concept and first scientific results, *J. Atmos. Sci.*, *56*, 151–175, 1999.

Chandrasekhar, S., *Radiative Transfer*, Oxford Univ. Press, New York, 1950. (Also: Dover, Mineola, N.Y., 1960.)

De Haan, J. F., P. B. Bosma, and J. W. Hovenier, The adding method for multiple scattering calculations of polarized light, *Astron. Astrophys.*, *183*, 371–391, 1987.

De Rooij, W. A., and C. C. A. H. Van der Stap, Expansion of Mie scattering matrices in generalized spherical functions, *Astron. Astrophys.*, *131*, 237–248, 1984.

Deschamps, P. Y., F. M. Bréon, M. Leroy, A. Podaire, A. Bricaud, J. C. Buriez, and G. Sèze, The POLDER mission: Instrument characteristics and scientific objectives, *IEEE Trans. Geosci. Remote Sens.*, *32*, 598–615, 1994.

Deutsche Forschungsanstalt für Luft- und Raumfahrt, GOME level 0 to 1 algorithms description, *Rep. ER-TN-DLR-GO-0022*, issue 3A, DLR/DFD, Oberpfaffenhofen, Germany, 1995.

European Space Agency (ESA), *GOME Users Manual*, *ESA SP-1182*, ESA/Eur. Space Res. and Technol. Cent., Noordwijk, The Netherlands, 1995.

Fischer, J., and H. Grassl, Detection of cloud-top height from backscattered radiances within the oxygen *A* band, part 1, Theoretical study, *J. Appl. Meteorol.*, *30*, 1245–1259, 1991.

Fischer, J., W. Cordes, A. Schmidz-Pfeiffer, W. Renger, and P. Mörl, Detection of cloud-top height from backscattered radiances within the oxygen *A* band, part 2, Measurements, *J. Appl. Meteorol.*, *30*, 1260–1267, 1991.

Hale, G. M., and M. R. Querry, Optical constants of water in the 200-nm to 200-μm wavelength region, *Appl. Opt.*, *12*, 555–563, 1973.

Hanel, R. A., Determination of cloud altitude from a satellite, *J. Geophys. Res.*, *66*, 1300, 1961.

Hansen, J. E., Multiple scattering of polarized light in planetary atmospheres, part 1, The doubling method, *J. Atmos. Sci.*, *28*, 120–125, 1971.

Hansen, J. E., and L. D. Travis, Light scattering in planetary atmospheres, *Space Sci. Rev.*, *16*, 527–610, 1974.

Hovenier, J. W., Multiple scattering of polarized light in planetary atmospheres, *Astron. Astrophys.*, *13*, 7–29, 1971.

Hovenier, J. W., and C. V. M. Van der Mee, Fundamental relationships relevant to the transfer of polarized light in a scattering atmosphere, *Astron. Astrophys.*, *128*, 1–16, 1983.

Kuze, A., and K. V. Chance, Analysis of cloud top height and cloud coverage from satellites using the O_2 *A* and *B* bands, *J. Geophys. Res.*, *99*, 14,481–14,491, 1994.

Lacis, A. A., and V. Oinas, A description of the correlated *k* distribution method for modeling nongray gaseous absorption, thermal emission, and multiple scattering in vertically inhomogeneous atmospheres, *J. Geophys. Res.*, *96*, 9027–9063, 1991.

McClatchey, R. A., R. W. Fenn, J. E. A. Selby, F. E. Volz, and J. S. Garing, Optical properties of the atmosphere, *Rep. AFCRL-72.0497*, Air Force Cambridge Res. Lab., Hanscom Air Force Base, Mass., 1972.

Mishchenko, M. I., and L. D. Travis, Satellite retrieval of aerosol properties over the ocean using polarization as well as intensity of reflected sunlight, *J. Geophys. Res.*, *102*, 16,989–17,013, 1997.

Nakajima, T. Y., T. Nakajima, M. Nakajima, H. Fukushima, M. Kuji, A. Uchiyama, and M. Kishino, Optimization of the Advanced Earth Observing Satellite II Global Imager channels by use of radiative transfer calculations, *Appl. Opt.*, *37*, 3149–3163, 1998.

Netherlands Organization for Applied Scientific Research-Institute of Applied Physics (TNO-TPD), *Polarization Properties of GOME FM*, issue 1, *ER-TR-TPD-GO-0028*, Delft, The Netherlands, 1994.

O'Brien, D. M., and R. M. Mitchell, Error estimates for retrieval of cloud-top pressure using absorption in the *A* band of oxygen, *J. Appl. Meteorol.*, *31*, 1179–1192, 1992.

Preusker, R., U. Böttger, and J. Fischer, Spectral and bidirectional measurements of the Stokes vector in the O_2 *A* band and their interpretation, *Proc. SPIE Int. Soc. Opt. Eng.*, *2582*, 13–20, 1995.

Rothman, L. S., et al., The HITRAN molecular database: Editions of 1991 and 1992, *J. Quant. Spectrosc. Radiat. Transfer*, *48*, 469–507, 1992.

Saiedy, F. H., H. Jacobowitz, and D. Q. Wark, On cloud-top determination from Gemini-5, *J. Atmos. Sci.*, *24*, 63–69, 1967.

Stam, D. M., J. F. De Haan, J. W. Hovenier, and P. Stammes, Degree of linear polarization of light emerging from the cloudless atmosphere in the oxygen *A* band, *J. Geophys. Res.*, *104*, 16,843–16,858, 1999.

Stam, D. M., J. F. De Haan, J. W. Hovenier, and P. Stammes, A fast method for simulating observations of polarized light emerging from the atmosphere applied to the oxygen *A* band, *J. Quant. Spectrosc. Radiat. Transfer*, *64*, 131–149, 2000.

Stammes, P., F. Kuik, and J. F. De Haan, Atmospheric polarization in the oxygen *A* and *B* bands, *Proc. Progr. Electromagn. Res. Symp.*, *1994*, 2255–2259, 1994.

Vanbauce, C., J. C. Buriez, F. Parol, B. Bonnel, G. Séze, and P. Couvert, Apparent pressure derived from ADEOS-POLDER observations in the oxygen *A* band over ocean, *Geophys. Res. Lett.*, *25*, 3159–3162, 1998.

Van de Hulst, H. C., *Light Scattering by Small Particles*, John Wiley, New York, 1957. (Also Dover, Mineola, N.Y., 1981.)

Van de Hulst, H. C., *Multiple Light Scattering: Tables, Formulas and Applications*, Academic, San Diego, Calif., 1980.

Wark, D. Q., and D. M. Mercer, Absorption in the atmosphere by the oxygen *A* band, *Appl. Opt.*, *4*, 839–845, 1965.

Wu, M.-L. C., Remote sensing of cloud-top pressure using reflected solar radiation in the oxygen *A* band, *J. Clim. Appl. Meteorol.*, *24*, 539 546, 1985.

Yamamoto, G., and D. Q. Wark, Discussion of the letter by R. A. Hanel on "Determination of cloud altitude from a satellite," *J. Geophys. Res.*, *66*, 3596, 1961.

I. Aben, Space Research Organization Netherlands (SRON), Sorbonnelaan 2, 3584 CA Utrecht, The Netherlands. (E.A.A.Aben@sron.nl)

J. F. De Haan and J. W. Hovenier, Department of Physics and Astronomy, Vrije Universiteit, De Boelelaan 1081, 1081 HV Amsterdam, The Netherlands. (johan@nat.vu.nl; hovenier@nat.vu.nl)

D. M. Stam, Department of Astronomy, Space Sciences Building, Cornell University, Ithaca, NY 14853. (stam@astrosun.tn.cornell.edu)

(Received September 20, 1999; revised April 5, 2000; accepted April 12, 2000.)